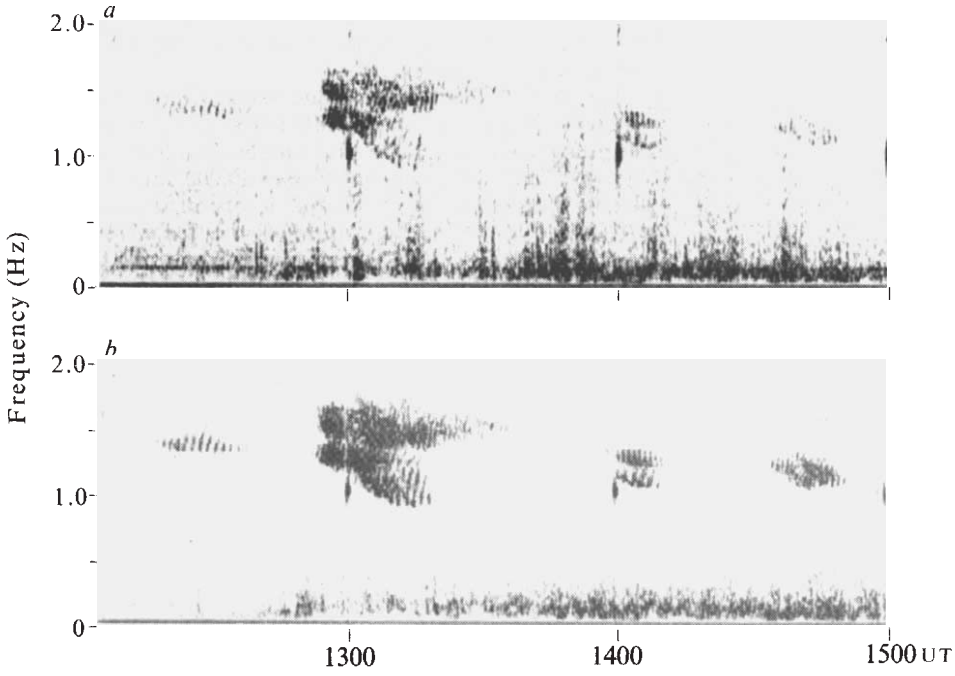

Fig. 1 Spectrograms of a series of Pc 1 geomagnetic pulsation events recorded at Stanford, California, using tree potentials (*a*) and a conventional solenoid antenna (*b*). Short intervals of a 1 Hz calibration signal appear at the start of each hour. The vertical lines in the upper spectrogram are caused either by local electromagnetic transients or by natural sferics; similar lines occur in the lower spectrogram, but they are not as obvious because the background noise is comparatively suppressed.

These results, and the observations of natural Pc 1 pulsations, can possibly be best understood by considering the tree/electrode pair combination to form a collection of conducting loop antennas in which e.m.fs may be induced by magnetic field fluctuations in the appropriate direction. The conducting paths are provided by the conducting material of the tree (and the cambium in particular[11]), and, for field fluctuations in a particular direction, the area of the relevant loop antenna is defined by the intersection of the tree with a vertical plane perpendicular to the particular field direction and passing through the two electrodes. Thus, in the measurements reported here, the Pc 1 pulsation events observed in the tree potentials were produced by Pc 1 pulsations of the north–south component of the geomagnetic field.

Further tests showed that the tree potentials could only be detected in a living tree. Thus, when a tree dies, the potentials gradually disappear as the wood dries and loses its conductivity.

In conclusion, measurements with tree electrodes show that trees may be used as 'antennas' to detect ULF geomagnetic pulsations. The measurements also show that ULF tree potentials are largely produced by ULF fluctuations of the geomagnetic field (the remaining component of the potentials is probably thermal noise). Presman[12] noted that electromagnetic fields usually have an adverse effect on living processes. If the ULF geomagnetic pulsations have any adverse effect on the growth of trees (and, as we have seen, they must induce electric currents in the living material) these effects could possibly be observed in tree ring data. Pc 1 geomagnetic pulsation occurrences vary markedly over a solar cycle[9] and thus, if these particular pulsations effect tree growth, a solar cycle in tree ring data could occur. LaMarche and Fritts[13] searched unsuccessfully for a relation between tree ring data and sunspot numbers. The phase of the Pc 1 pulsation solar cycle, however, differs by several years from the sunspot cycle and, assuming the two cycles affect tree ring data, they may tend to obscure each other's effects. Furthermore, other geomagnetic pulsations and higher-frequency electromagnetic signals have their own cycles of occurrence, and their effects on tree ring formation, if any, could add further to the complexity of the tree ring data. Studies of these possible effects are desirable, because the tree ring data could provide a unique record of past ULF and higher-frequency geomagnetic activity.

I thank D. B. Coates for technical assistance. This work was supported in part by the Advanced Research Projects Agency of the US Department of Defence and in part by the US Office of Naval Research.

A. C. Fraser-Smith

Radioscience Laboratory,
Stanford Electronics Laboratories,
Stanford University,
Stanford, California 94305

Received 16 August; accepted 15 December 1977.

1. Jacobs, J. A. *Geomagnetic Micropulsations* 15 (Springer, New York, 1970).
2. Campbell, W. H. *Proc. IEEE* **51**, 1337–1342 (1963).
3. Tepley, L. R. *J. geophys. Res.* **66**, 1651–1658 (1961).
4. Lokken, J. E., Shand, J. A. & Wright, C. S. *J. geophys. Res.* **68**, 789–794 (1963).
5. Lokken, J. E. in *Natural Electromagnetic Phenomena Below 30 Kc/s* (ed. Bleil, D. F.) 373–428 (Plenum, New York 1964).
6. Buxton, J. L. & Fraser-Smith, A. C. *IEEE Trans. Geosci. Elec.* **GE-12** 109–113 (1974).
7. Troitskaya, V. A. *J. geophys. Res.* **66**, 5–18 (1961).
8. Heacock, R. R. & Hessler, V. P. *J. geophys. Res.* **67**, 3985–3995 (1962).
9. Fraser-Smith, A. C. *J. geophys. Res.* **75**, 4735–4745 (1970); *J. geophys. Res.* **77**, 4209–4220 (1972).
10. Fraser-Smith, A. C. & Coates, D. B. *Radio Sci.* (submitted).
11. Burr, H. S. *Yale J. Biol. Med.* **17**, 727–734 (1945); *Yale J. Biol. Med.* **19**, 311–318 (1947); *Science* **124**, 1204–1205 (1956).
12. Presman, A. S. *Electromagnetic Fields and Life* (transl. Sinclair, F. L., ed. Brown, F. A. Jr) 155 (Plenum, New York, 1970).
13. LaMarche, Jr, V. C. & Fritts, H. C. *Tree-Ring Bull.* **32**, 19–33 (1972).

Mass spectrometric measurement of the positive ion composition in the stratosphere

The ion composition of the upper atmosphere has been the subject of many experiments. Early mass spectrometer measurements have been primarily concerned with the ion composition at altitudes between 60 and 250 km (refs 1–6). Few data, however, are available on the charged particle composition of the stratosphere. Global ion density measurements using electric probes[7–11] indicate number densities of the order of 100–10,000 cm^{-3} for positive ions in this region. Arnold *et al.*[12] have recently published the first mass spectrometric data of the stratospheric ion composition, obtained on the downleg portion of three rocket flights. Above 40 km they observe the proton hydrates as being the most abundant ions. Below 40 km a change in the predominant ion species is seen, which is explained by Arnold *et al.* by ion molecule reactions between water cluster ions and

0028–0836/78/0271—0642$01.00

formaldehyde. One of the possible dangers, inherent to rocket flights, however, is the alteration of the ion composition, due to shock wave-induced fragmentation. Mass spectrometric measurements on this region using a balloon-borne instrument were suggested[13] as early as 1969. Here we give the first preliminary results of a successful flight, performed with a balloon-borne quadrupole mass spectrometer on 30 September 1977. A 100,000 m³ Zodiac balloon was flown at mid-latitude (CNES lauching site at Aire sur l'Adour, France, 44 °N) at 18.27 UT and reached the altitude of 35 km at 20.00 UT. The measurements were started at 20.14 UT, which is after sunset.

The gondola, which will be described in more detail elsewhere, primarily consists of a high-speed helium cryopump, in which is built a quadrupole mass filter, followed by a high gain electron multiplier. The ions were sampled through a 0.2mm hole in a 0.1mm thickness stainless steel flange, which can be biased with respect to the gondola structure. Signal detection is realised

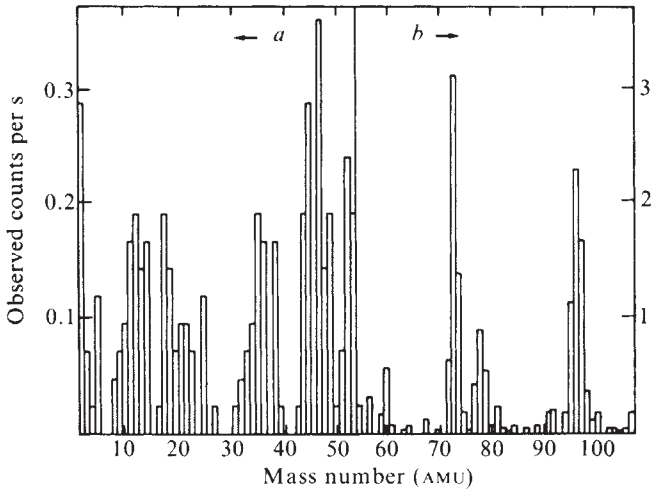

Fig. 1 Observed count rate versus mass number measured at 35 km altitude. Both *a* and *b* have been obtained by averaging of the counts observed, during seven scans. The applied draw-in-potential was −13 V.

by both analogue and pulse counting techniques. The mass spectrometer covers the mass range from 0 to 109 AMU. Measuring in mass domains as well as sweeping the complete mass range is possible[11]. Sweeping the complete mass range was realised by using discrete steps approximately 1 AMU in size. The integration time for pulse counting was 6 s per step. Thus spectra were obtained in the form of a histogram, as is shown in Figs 1 and 2. A fixed resolution mode was used throughout all scans reported here. Two separate draw-in-potentials were used, −13 and −4.6 V. Figure 1 represents the results obtained at −13 V and Fig. 2 those at −4.6 V. It should be noted that in both figures the number of observed counts per second for masses smaller than 55 AMU have been represented with a different scale factor. The count rate due to noise pulses was smaller than $0.1 s^{-1}$ during the whole flight.

The mass numbers of the detected ions are listed in Table 1, with the draw-in-potentials and the uncertainty in atomic mass numbers. Counts below mass 10 have not been taken into account, because instabilities have been observed in the power supply of the quadrupole for such low mass values.

As can be seen from Table 1, the uncertainty for lower mass numbers is rather high for two reasons. First, the fixed resolution, chosen rather low in favour of high sensitivity, gives rise to much more broadened peaks at lower masses, than at higher ones. Second, due to the low counting rate at low mass numbers, it was impossible to build up a complete histogram even after several scans and thus a faulty conclusion may be drawn about

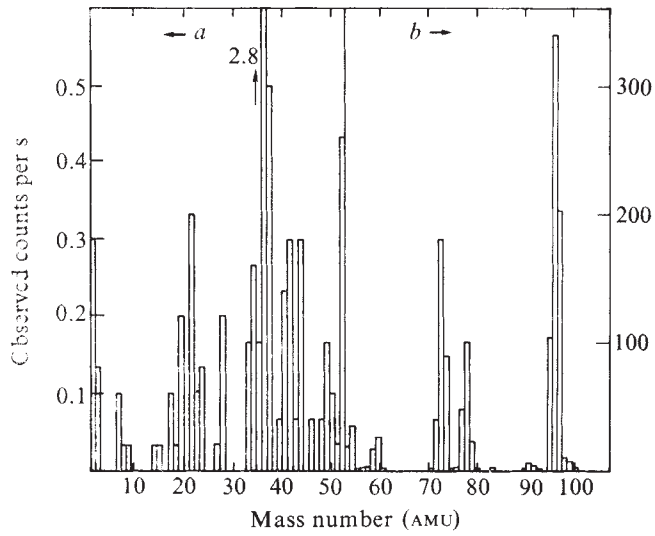

Fig. 2 Observed count rate versus mass number at 35 km altitude. *a*, The result of five scans; *b*, two scans. Applied draw-in-potential was −4.6 V.

the exact position of the pass peaks. Above mass 50, however, the signal was strong enough to permit a higher degree of certainty. Furthermore, the mass domain from 50 to 109 AMU has been scanned with a higher resolution and the results confirm those of Table 1. Masses 19 (18±3 and 20±3), 37, 55, 73 and 109 can be identified with the cluster ions $H^+(H_2O)_n$, n ranging from 1 to 6.

In all spectra, mass 73 was the most abundant peak among the water cluster ion peaks. The observed distribution of the $H^+(H_2O)_n$ cluster ion peaks is represented in Table 2.

Table 2 does not represent a correct number density distribution of the hydrated hydronium ions, as a correction factor has to be taken into account to convert peak height to number density (even on relative scale). The result of this correction, which is not known exactly and which cancels the effect of lower transmission of the mass filter at higher mass numbers, will be a larger percentage of mass 91. As possible cluster breaking up due to electric fields must also be considered, our results are difficult to compare with the distribution calculated by Mohnen[15].

It is not completely clear why the distribution of $H^+(H_2O)_n$ is different at different draw-in-potentials, although again electric field-induced breaking up of the cluster ions may have an important role.

Apart from the water cluster ions, which are expected according to the known reaction schemes[16], additional peaks

Table 1 Observed mass numbers

Draw-in-potential	
−13 V	−4.6 V
13±3	—
18±3	20±3
25±3	—
—	29±3
37±3	37±2
—	43±3
47±3	50±3
55±2	55±2
60±2	60±2
73±2	73±2
78±2	78±2
91±2	91±2
96±2	96±2
109±2	—

Table 2 Observed distribution of $H^+(H_2O)_n$ mass peaks at 35 km in %

n	Mass number	Draw-in-potential −15 V	−4.6 V
2	37	5	1
3	55	6	16
4	73	79	80
5	91	5	3
6	109	5	—

have been observed, among which 96±2 was the most abundant. At low draw-in-potentials, this peak was even larger than the one at mass 73. Masses 29, 42, 60 and 80 have also been observed by Arnold *et al.*[12], but they do not mention mass 96±2, nor do they report that they have observed masses 73, 91 and 109. Because this (96±2) is the most abundant mass peak among the non-proton hydrates which we have observed, it is tempting to conclude that rocket-borne measuring devices are more disturbing than balloon-borne instruments. However, care must be taken, as the ion-molecule reaction channels might be different during night time. The observed mass peaks can be partly fitted into the formaldehyde ion chemistry if 47±3 and 50±3 are tentatively identified as $H^+(CH_2O)H_2O$ and 96±2 as $H^+(CH_2O)_2(H_2O)_2$ or $C_2H_2O^+(H_2O)_3$. But, one should be careful because although the existence of formaldehyde in the stratosphere has been predicted theoretically[17], to our knowledge no experimental observation of it has been published. Furthermore, no reaction rate constants of formaldehyde ions or molecules with proton hydrates have been published. Thus any tentative identification must be regarded as speculative. As an alternative interpretation, however, mass numbers 60, 78 and 96 can be tentatively assigned to the hydrates of N_3^+, namely $N_3^+(H_2O)$, $N_3(H_2O)_2$ and $N_3^+(H_2O)_3$, respectively, which have already been observed in laboratory air flow discharges by Hayhurst and Padley[18]. In view of this, 47±3 and 50±3 may be interpreted as due to O_3^+.

We need more data, especially higher resolution mass spectra and conclusive laboratory work, before any final conclusions can be made. It is clear, however, from the observations reported here and from those of Arnold[12], that apart from the hydrated hydronium ions some other unknown ionic species are present in the stratosphere. This should give a new motivation for more extended laboratory and *in situ* investigations on the ionic chemistry of the stratosphere.

We thank Ir. C. Lippens and the technical staff of the Belgian Institute for Space Aeronomy, who made this experiment possible and Drs M. Ackerman and G. Kockarts for helpful criticisms.

E. Arijs
J. Ingels
D. Nevejans

Belgian Institute for Space Aeronomy, 3 Ringlaan, B-1180 Brussels, Belgium

Received 25 October; accepted 15 December 1977.

1. Johnson, C. Y. *Ann. Geophys.* **17**, 100–108 (1961).
2. Istomin, V. G. *Proc. Int. Space Sci. Symp. 3rd* 209–220 (1963).
3. Istomin, V. G. & Pokhunov, A. A. *Proc. Int. Space Sci. Symp. 3rd* 117–131 (1963).
4. Narcissi, R. S. & Bailey, A. D. *J. geophys. Res.* **70**, 3687–3700 (1965).
5. Narcissi, R. S., Bailey, A. D., Wlodyka, L. F. & Philbrick, C. R. *J. atmos. terr. Phys.* **34**, 647–658 (1972).
6. Krankowsky, D., Arnold, F., Wieder, H. & Kissel, J. *Int. J. Mass Spectrom. Ion Phys.* **8**, 379–390 (1972).
7. Hale, L. C., Hoult, D. P. & Baker, D. C. *Scient. Rep.* No. 223, Pennsylvania State Univ. (1967).
8. Mitchel, J. D., Hale, L. C., Olsen, R. O., Randawa, J. S. & Rubio, R. *Aeron. Rep.* **48** (1972).
9. Pedersen, A. & Kane, A. J. in *Mesopheric Models and Related Experiments* (ed. Fiocco) 274–278 (Reidel, Dordrecht 1971).
10. Smirnykh, L. N. *Cosmic Res.* **14**, 145–148 (1976).
11. Rose, G., Widdel, H. U., Azcarraga, A. & Sanchez, R. *Planet. Space Sci.* **20**, 871–876 (1972).
12. Arnold, F., Krankowsky, D. & Marien, K. H. *Nature* **267**, 30–32 (1977).
13. Ackerman, M. *et al. Aeronomica Acta C* **24** (1969).
14. Arijs, E. & Nevejans, D. *Rev. Scient. Instrum.* **46**, 1010–1015 (1975).
15. Mohnen, V. A. *Pure appl. Geophys.* **84**, 141–153 (1971).
16. Ferguson, E. E. in *The Natural Stratosphere of 1974*, CIAP Monograph 1, 5.42–5.54 (1974).
17. Stewart, R. W. & Hoffert, M. I. *J. atmos. Sci.* **32**, 195–210 (1975).
18. Hayhurst, A. N. & Padley, P. J. *Trans. Faraday Soc.* **63**, 1620–1630 (1967).

Chemical interpretation of Viking Lander 1 life detection experiment

Preliminary results of the Viking Lander 1 (VL-1) biology experiments[1] revealed that humidification of the martian soil sample in the gas exchange experiment (GEX) released substantial amounts of carbon dioxide and oxygen, as well as detectable amounts of nitrogen and argon or carbon monoxide. We have reviewed the available flight data and found that, when the amounts of evolved gases were plotted in an adsorption potential plot, the amount of evolved oxygen was anomalously high compared to the other gases. This paper also describes simulation experiments with a model Mars soil provided by the Viking Inorganic Analysis Team (ICAT) and treated with a radiofrequency (RF) glow discharge in a simulated martian atmosphere. The findings indicated that the GEX simulation procedure released oxygen, carbon dioxide, and nitrogen in amounts comparable to that seen in the experiment on Mars.

The design of the GEX and its modes of operation have been described elsewhere[2]. The values first reported[1] have been revised, and the maximum amounts of gases evolved from the entire 1 cm^3 of humidified sample in the test cell have been given by Oyama *et al.*[3] as 83 nmol N_2, 775 nmol O_2, 9,800 nmol CO_2, and 13 nmol Ar/CO. Ar and CO were not separated in the chromatographic column.

The postulate considered here for the gas evolved in the VL-1 humid mode GEX was that the amount of gas seen could have been physically or chemically adsorbed, or attached in a surface complex, on the martian soil. Using a molecular area of 14.6×10^{-20} m^2 for O_2 and an estimated bulk density of soil sample of 1.3 g cm^{-3}, it can be calculated that the evolved O_2 would cover an area of 0.052 m^2 g^{-1} soil. The estimated bulk density was the same value as that used in ref. 3 and was the midpoint of the range estimated in ref. 4 from the observed physical behaviour of the fine-grained materials in the immediate vicinity of VL-1. A similar calculation for the CO_2, using a molecular area of 17×10^{-20} m^2, gives a surface coverage 0.77 m^2 g^{-1}. A specific surface area of 1 m^2 g^{-1} or greater could, therefore, have accommodated the evolved O_2 and CO_2.

Fig. 1 Adsorption potential plot of gas evolved in VL-1 GEX humid mode experiment. The 'A value' ordinate includes sample temperature, T, in K, molar volume of liquid adsorbate, V_m, in cm^3 g^{-1}, and the reciprocal of the relative vapour pressure of the adsorbate, P_0/P where $A = (T/V_m)\log_{10}(P_0/P)$. ◇, CO; ○, O_2; □, CO_2; △, N_2; ▽, Ar.

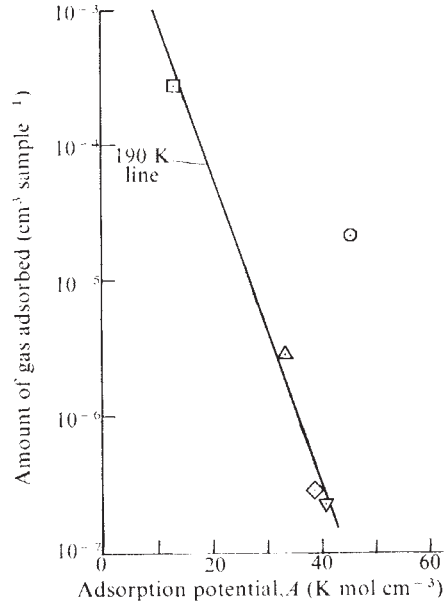

0028-0836/78/0271-0644$01.00